

Three-dimensional structure of system I of photosynthesis at 6 Å resolution

Norbert Krauss*, Winfried Hinrichs*, Ingrid Witt*†, Petra Fromme†, Wolfgang Pritzkow*, Zbigniew Dauter‡, Christian Betzel‡, Keith S. Wilson‡, Horst T. Witt† & Wolfram Saenger*

* Institut für Kristallographie, Freie Universität Berlin, Takustrasse 6, 1000 Berlin 33, Germany

† Max-Volmer-Institut für Biophysikalische und Physikalische Chemie, Technische Universität Berlin, Strasse des 17. Juni 135, 1000 Berlin 12, Germany

‡ European Molecular Biology Laboratory Outstation at DESY, Notkestrasse 85, 2000 Hamburg 52, Germany

X-ray structure analysis shows that the monomer of trimeric photosystem I (PS I) of *Synechococcus* sp. consists of a catalytic domain and a smaller domain that connects the monomers. The 4Fe–4S clusters F_X , F_A and F_B , 28 α -helices and 45 chlorophyll *a* molecules were located. The two large subunits of PS I are represented by nine α -helices each; they are related by a local 2-fold rotation axis passing through F_X . Electron densities close to this axis are interpreted as carriers of the electron transfer chain.

PHOTOSYNTHESIS converts light energy into chemical energy stored in the synthesized organic material. In water-oxidizing photosynthesis, that is in higher plants and cyanobacteria, the primary conversion takes place through light-induced transmembrane charge separations at the reaction centres of photosystems I and II (PS I and PS II). At PS II this takes place by an electron transfer from water at the inner side of the membrane (lumen) to a plastoquinone, Q_A , at the outer side (stroma). From there the electron is translocated together with a proton across the membrane through a pool of plastoquinones, a cytochrome b_6/f protein complex and plastocyanin, PC, to the inner side of PS I. At PS I the electron is transferred across the membrane to the outside, where ferredoxin accepts the electron and transports it to NADP⁺ reductase.

The vectorial electron transfer and the subsequent proton translocations generate an electrochemical potential across the membrane, which drives ATP synthesis. The products of these primary reactions, NADPH and ATP, are used in the dark reactions to reduce CO₂ to carbohydrates (for review see ref. 1).

Although the reaction centre of photosynthetic purple bacteria with known three-dimensional structure^{2,3} is not able to oxidize water, it displays important similarities to that of PS II^{3,4}. In contrast, the reaction centre of PS I is related to that in photosynthetic green sulphur bacteria^{5,6}, but structural information of PS I at the atomic level is not available. Recently, the genes of the 11 subunits of the thermophilic cyanobacterium *Synechococcus* sp. were sequenced^{7,8}. PS I contains two large (A, B of $M_r \sim 83K$) and five small (I, J, K, L, M of 3–15K) membrane intrinsic subunits; in this notation, A corresponds to the gene product psaA; B to psaB and so on. Further subunits C, D, E, (8–16K) are located on the stromal side and F (15K) on the luminal side of the membrane. The total M_r of PS I including 90 antenna chlorophylls is 340K.

In PS I, charge separation starts with the photooxidation of the pigment P700 at the luminal side, which may be present as a chlorophyll *a* dimer^{9–12}. The released electron moves through A_0 (chlorophyll *a*)¹³ and A_1 (vitamin K₁)^{14,15} to the first 4Fe–4S cluster, F_X , which is bound to the two large subunits A and B. From F_X , the electron is transferred to two other 4Fe–4S clusters F_A and F_B , which are coordinated to subunit C on the stromal side of PS I^{16,17}. Here ferredoxin probably takes over the electron for transport to NADP⁺ reductase¹².

The crystallization and X-ray characterization of PS I from different species have been described^{18–23}. Crystals of PS I from *Synechococcus* sp. are suitable for X-ray structure analysis to 4 Å resolution^{21,24}; here we present the three-dimensional struc-

ture of this PS I at 6 Å resolution. Experimental details are given in Table 1; the overall structure of PS I and its division into two domains are described in Fig. 1a–c; sections of the electron density map and their interpretation are shown in Fig. 2a–c.

Structural elements

4Fe–4S clusters. In the electron density map (Fig. 2a), there are three spherical maxima with density 12 root-mean-square (r.m.s.) deviations above the mean density. They were assigned to the three clusters F_X , F_A and F_B .

α -Helices. The electron density map contains many tubular structures. They were interpreted as α -helices and fitted with polyalanine α -helices (Fig. 2b) in arbitrary axial orientation, because at 6 Å resolution the polarity of the α -helices cannot be determined. The α -helices have not been connected by polypeptide segments because the limited resolution did not permit continuous tracing.

Chlorophyll *a*. The electron density map shows numerous disk-like, ellipsoidal globules of 8–10 Å diameter and 4–5 Å thickness. These densities were interpreted as the dihydroporphyrin systems of chlorophyll *a* (Fig. 2b, c). The flattened shape of these disks allowed estimation of their orientation in space, but the rotation within their plane is arbitrary.

Iron–sulphur clusters

The three 4Fe–4S clusters are arranged in the form of an irregular triangle (Figs 2a, 3a, 4a). Its plane roughly passes through the crystallographic 3-fold and local 2-fold axes (Fig. 3b–d). The electron density closest to the membrane sheet can be attributed to F_X , which is supposed to coordinate the membrane-integrated subunits A and B with two cysteines each¹². The densities of the other two, F_A and F_B , are 14 and 21 Å from F_X , respectively (Fig. 4); distinction between F_A and F_B cannot be made. The comparable electron densities of F_X , F_A and F_B contradict the notion that one of the clusters occurs as 2Fe–2S (ref. 25) and supports recent data that are in favour of three 4Fe–4S (refs 26, 27).

We have compared the distance between F_A and F_B (12 Å), which are coordinated to the ferredoxin-like subunit C, with that of the two 4Fe–4S clusters in the known three-dimensional model of bacterial ferredoxin^{28,29} from *Peptococcus aerogenes*. Although the polypeptides of the two proteins are different, there is structural analogy because the distances between the two 4Fe–4S clusters are identical. Because this is expected to lead to similar electron transfer rates, provided the polarities of

the redox centre environments and free energies are roughly comparable³⁰, the electron transfers of bacterial ferredoxin and subunit C of PS I may be functionally related.

Arrangement of α -helices

The large number of 28 identified α -helices is in agreement with circular dichroism (CD) spectroscopic studies, which predicted PS I from algae to contain about 55% α -helical and only 7% β -sheet structure³¹. Although most of the α -helices are straight, some are kinked and made up of two pieces (Fig. 3). Most of the helices are of the transmembrane type, as predicted for PS I¹² and oriented at an angle between 3° and 30° to the membrane normal. Seven helices are nearly parallel to the membrane layer, and located towards the stromal or luminal side.

Looking onto the plane of the membrane (Fig. 3d), an elongated array of helices is recognized. Eight transmembrane helices (*a* to *h*) are symmetrically related with eight other helices (*a'* to *h'*) so that *a* corresponds to *a'*, *b* to *b'*, and so on. This defines a local roughly 2-fold rotation axis passing through F_x . We assign these blocks to subunits A and B because of the high homology of their amino-acid sequences⁷, and because of the folding into a comparable pattern of 11 helices each, as deduced tentatively from hydrophathy profiles⁸. The hydrophathy profile of subunit A indicates a unique long α -helix⁸. Because the kinked helix *g* is by far the longest in the array, we tentatively assign α -helices (*a* to *h*) to subunit A. The division of the array of helices into two blocks (*a* to *h* and *a'* to *h'*) is based on their 'obvious' spatial separation, but other divisions which still obey the approximate symmetry are possible: for example, A (*a* to *d*, *e'*, and *f*, *g*, *h*) and B (*a'* to *d'*, *e*, and *f'*, *g'*, *h'*).

On the luminal side there are two further helices (*n*, *n'*) (Fig.

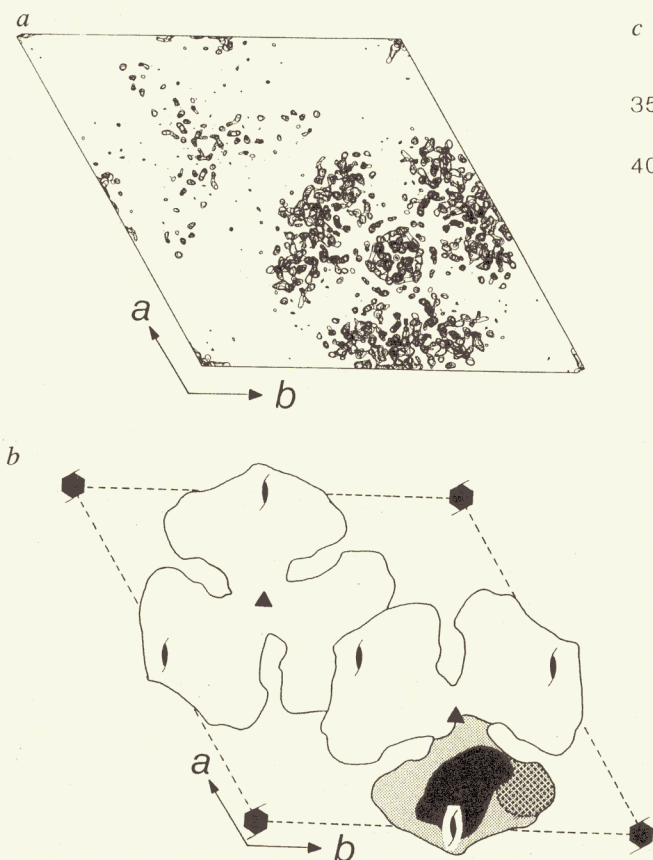


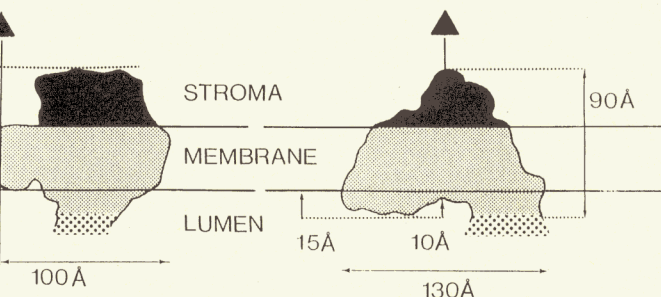
FIG. 1 *a*, Electron density map. 'Top' view onto the crystallographic *a*, *b*-plane, which is assumed to be parallel to the membrane layer. Shown is a section of 28 Å thickness, which contains a region of the membrane embedded part of the PS I complex. The contours are drawn at a level 2 r.m.s. deviations above the mean density. *b*, Packing of the PS I trimers in the crystal unit

cell with an 11 Å shortest separation between their axes, which are also related by the local symmetry and probably belong to subunits A and B. Helices (*i*, *j*, *k*, *l*, *m*) have no symmetry equivalent (Fig. 3d). Helix *i* is connected by electron density to the stromal side of PS I. It cannot belong to the stroma subunits C, D or E, because these can be removed by chaotropic reagents and are probably not anchored by a membrane-intrinsic helix¹². Helix *i* could perhaps belong to subunit J, which has an amino-terminal transmembrane helix and a hydrophilic region at the carboxy terminus.

Because *j* and *k* are linked by electron density, they are presumably part of subunit K, which possibly consists of two α -helices^{7,8}. Helices *j* and *k* are close to the 3-fold axis in a tight bundle which might be responsible for the organization of the monomers into the trimeric form. For helices *l*, *m* and the additional helices on stromal and luminal sides (white helices only shown in Fig. 3a-c), no definite assignment can be made.

Arrangement of chlorophyll *a* molecules

Most of the identified 45 chlorophyll *a* molecules are oriented with their dihydroporphyrin planes roughly perpendicular to the membrane (Fig. 3a, b), similar to those observed in the light-harvesting complex II (LHC II)³² and as predicted by linear dichroism spectroscopic studies³³. Some of the chlorophyll *a* molecules belong to the electron transfer chain, all others to the antenna system. The latter are located around the transmembrane helical core of the subunits A, B (see Fig. 3a, b). The distances between centres of neighbouring dihydroporphyrins of most of these light-harvesting chlorophyll *a* are 8 to 15 Å, similar to those reported for other light-harvesting complexes^{32,34}. Several of the closely spaced chlorophyll *a* form



cell with symmetry elements indicated in the same view as in *a*. One monomer is shaded, with stromal part black, membrane-embedded part light, and luminal, less well ordered part dotted. The separation line between the monomers is drawn arbitrarily. *c*, View onto one PS I monomer. Left, view direction down the crystallographic *b*-axis for the monomer which is shaded in *b*. Right, view direction perpendicular to the crystallographic *b*, *c*-plane. *a*, *b*, Arrangement of the PS I trimer in the unit cell. The tripartite disk with ~100 Å radius is centred on the crystallographic 3-fold axis. Each of the three identical monomers is divided into a small and a large domain (*c*, left) which are connected by narrow sections of electron density (*a*). The smaller 'connecting' domains with ~40 Å height and ~30 Å width are so close to the 3-fold axis that they appear to be engaged in trimerization. The larger 'catalytic' domain with 130 Å length and 70 Å width harbours the electron transport chain (see below). Because most of the 28 helices that were identified are oriented roughly parallel to the *c*-axis and located within a sheet parallel to the *a*, *b*-plane (Fig. 2a), which is ~40 Å thick (see below) as commonly observed for biological membranes⁴⁴, we associate this sheet with the membrane-embedded part of PS I (*c*). We can also identify the stromal and luminal sides of the PS I trimer, because the three 4Fe-4S clusters of PS I are known to be located on the stromal side¹¹ and have been found within the 35 Å-high 'hump' protruding from the large domain (black in *b*, *c*). On the luminal side of the large domain, there is a 10 Å depression. On one side of this depression, a large portion of partly connected, less well defined electron density is found (dotted in *b*, *c*). A similar outer structure of PS I has previously been observed also by electron microscopy⁴⁵⁻⁴⁹, but the partition into two domains was not obvious. Possibly, the observed trimer also occurs *in vivo*^{50,51}. In solution, the trimer has been dissociated into dimers and monomers⁴⁸. Because each of the monomer contains one photocentre P700, it represents the PS I.

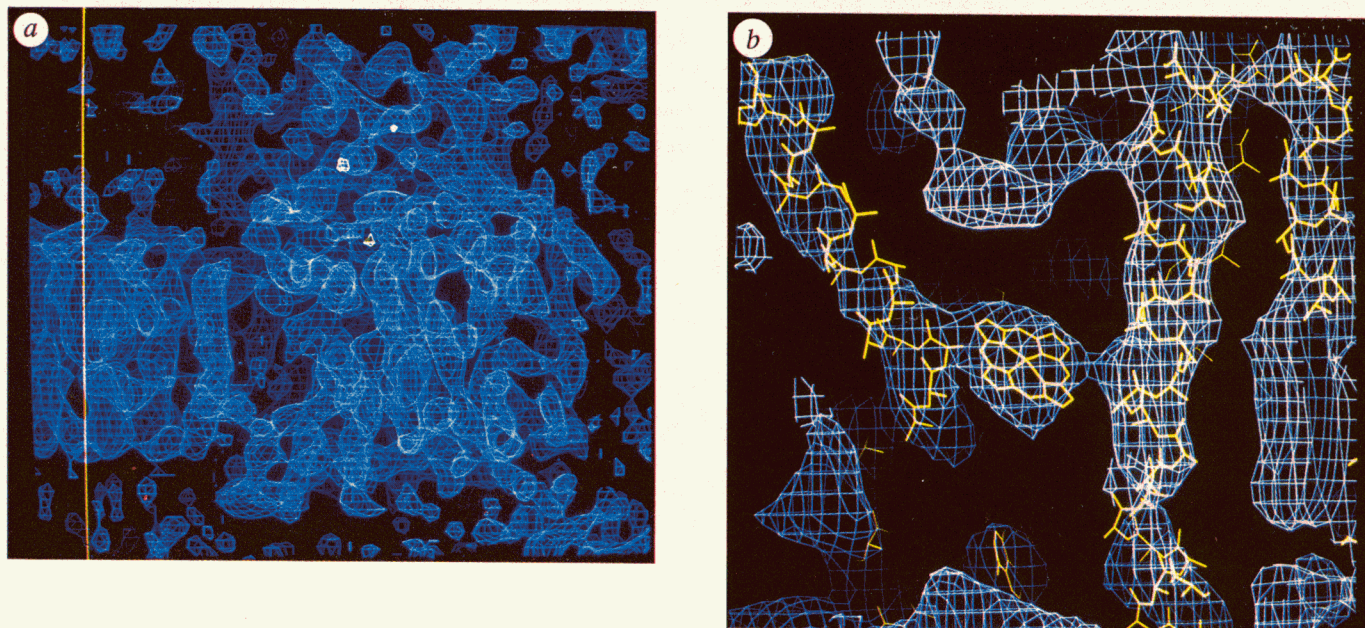


TABLE 1 Data collection and phasing statistics

Data collection

| Data | Number of crystals | Resolution (Å) | Number of measurements | Unique reflections (% completeness) | R_{merge}^{\S} |
|--|--------------------|----------------|------------------------|-------------------------------------|-------------------------|
| Native* | 2 | 20.0–6.0 | 49,832 | 18,703 (94.0) | 0.070 |
| EMTS (1)*† | 1 | 20.0–6.0 | 35,568 | 17,103 (89.8) | 0.101 |
| EMTS (2)*† | 2 | 20.0–6.0 | 64,035 | 17,714 (91.7) | 0.058 |
| PIP*† | 2 | 20.0–6.0 | 48,973 | 17,657 (91.6) | 0.130 |
| $\text{K}_3\text{UO}_2\text{F}_5^{\ddagger}$ | 1 | 20.0–9.0 | 5,577 | 3,873 (72.4) | 0.063 |

Phasing statistics

| Derivative | Anomalous data | Number of sites | $R_{\text{deriv}}^{\parallel}$ | $R_{\text{Cullis}}^{\nabla}$ | Phasing power (resolution (Å)) |
|-----------------------------------|----------------|-----------------|--------------------------------|------------------------------|--------------------------------|
| EMTS (1) | yes | 3 | 0.151 | 0.655 | 1.70 (6.0) |
| EMTS (2) | yes | 4 | 0.097 | 0.672 | 1.71 (6.0) |
| PIP | yes | 5 | 0.185 | 0.737 | 1.54 (6.0) |
| $\text{K}_3\text{UO}_2\text{F}_5$ | no | 2 | 0.127 | 0.614 | 1.03 (9.0) |

Mean figure of merit as a function of resolution (20–6 Å)

| Resolution range (Å) | 15.48 | 12.63 | 10.67 | 9.23 | 8.14 | 7.27 | 6.58 | 6.00 | total |
|-----------------------|-------|-------|-------|-------|-------|-------|-------|-------|--------|
| Number of reflections | 619 | 966 | 1,378 | 1,895 | 2,472 | 3,109 | 3,829 | 4,435 | 18,703 |
| Mean figure of merit | 0.75 | 0.76 | 0.75 | 0.73 | 0.69 | 0.67 | 0.61 | 0.54 | 0.65 |

Synechococcus sp. PS I was isolated and purified in trimeric form as described¹⁹. Crystallization of the trimers was done by the reverse of the 'salting in' procedure. For this, the salt concentration in a solution containing 30 mg ml⁻¹ protein, 100 mM MgSO₄, 5 mM 2-(*N*-morpholino)ethanesulphonic acid, pH 6.4, 0.02% w/w β-dodecylmaltoside was slowly reduced within 1–2 days through dialysis against the same buffer with lower salt concentration. At about 6 mM MgSO₄, crystallization takes place²⁴. Crystals grow as hexagonal, dark green prisms (1–2 mm long and 0.5 mm wide). Because the X-ray reflections obtained from these crystals are closely spaced owing to the large hexagonal unit cell with $a=b=287$ Å and $c=167$ Å, and diffuse owing to a relatively large mosaic spread ($\sim 0.5^\circ$), interpretable diffraction patterns could only be obtained with the intense and well collimated radiation from synchrotron sources (see below). The space group is $P6_3$ with two PS I trimers in the unit cell or one PS I monomer in the asymmetric unit. On this basis, the solvent content including detergent is calculated to be 78%. The crystal structure was determined by multiple isomorphous replacement including anomalous dispersion effects. X-ray diffraction data were collected at room temperature (20 °C) * with an image plate detector at the EMBL-outstation (DESY, Hamburg/Germany), $\lambda=0.96$ Å, and † with a FAST detector from Enraf-Nonius, Delft/Holland at SRS (Daresbury/United Kingdom), $\lambda=0.89$ Å. Wavelengths around 1 Å were chosen to prolong the lifetime of the crystals in the X-ray beam. Image plate data were processed using MOSFLM (Imperial College, London) and CCP4³⁹ programs. FAST data were processed using MADNES⁴⁶ and scaled in 3° batches. The x, y coordinates of all the heavy atoms were derived from difference Patterson maps. Because space group $P6_3$ is polar, the z -coordinate of one position of the EMTS(1) derivative was set to $z=0$, and the z -coordinates of the other positions were obtained from the Patterson cross-peaks. These coordinates were used to calculate cross-phase difference Fourier maps of the other heavy-atom derivatives, and the corresponding heavy-atom positions were located. Heavy-atom parameters were refined against centric data, initial phase angles were calculated using PHARE (mean figure of merit 0.65) and served to calculate an electron density map. The phase angles were improved considerably by eight cycles of solvent flattening⁴¹ (mean figure of merit 0.80) using a conservative solvent content of 75% and a 22 Å averaging radius to calculate the protein molecular envelope with the reciprocal-space equivalent⁴² of B. C. Wang's algorithm⁴¹. The electron density map calculated from these improved phases was interpreted with FRODO⁴³ on an Evans & Sutherland ESV display unit. The atomic coordinates will be deposited with the Brookhaven Protein Data Bank. † EMTS, sodium-2-ethylmercurithiosalicylate; PIP, Bis(μ -iodo-ethylenediamine)platinum(II)nitrate. Heavy-atom derivatives were prepared by soaking crystals at 1 mM concentrations of the respective compounds for 24 h (EMTS(1) and PIP) and 12 h (EMT(2)); $\text{K}_3\text{UO}_2\text{F}_5$ was at 1 mM and 20 h soak time. § $R_{\text{merge}} = \sum_n \sum_i |I_i - \langle I \rangle| / \sum_n \sum_i I_i$; where I_i are intensity measurements of a reflection and $\langle I \rangle$ is the mean intensity of this reflection. || $R_{\text{deriv}} = \sum |F_{\text{PH}} - F_{\text{P}}| / \sum |F_{\text{P}}|$; where F_{PH} and F_{P} are structure amplitudes of derivative and native crystal, respectively. ¶ $R_{\text{Cullis}} = \sum ||F_{\text{PH}}(\text{obs}) \pm F_{\text{P}}(\text{obs}) - F_{\text{H}}(\text{calc})|| / \sum |F_{\text{PH}}(\text{obs}) - F_{\text{P}}(\text{obs})|$; for centric reflections. # Phasing power is defined as $F_{\text{H}}(\text{r.m.s.})/E(\text{r.m.s.})$; where $F_{\text{H}}(\text{r.m.s.})$ are the r.m.s. heavy-atom structure factor amplitudes and $E(\text{r.m.s.})$ are the r.m.s. residual lack of closure errors.

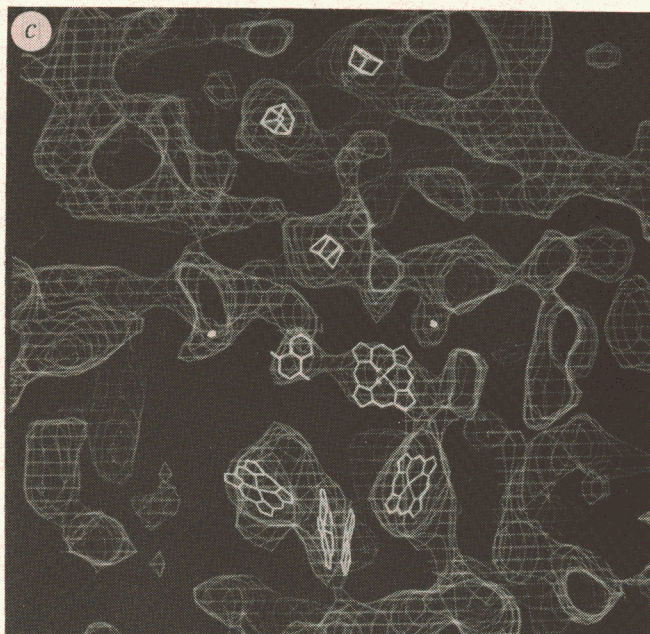
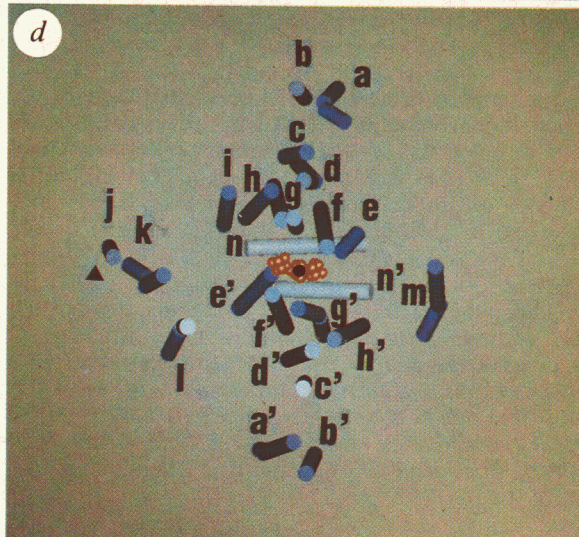
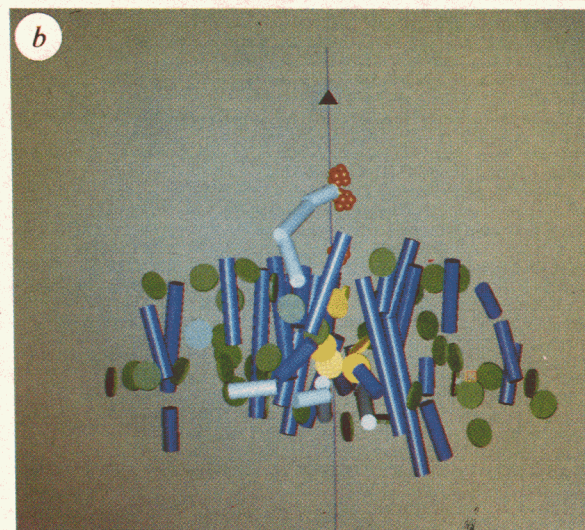
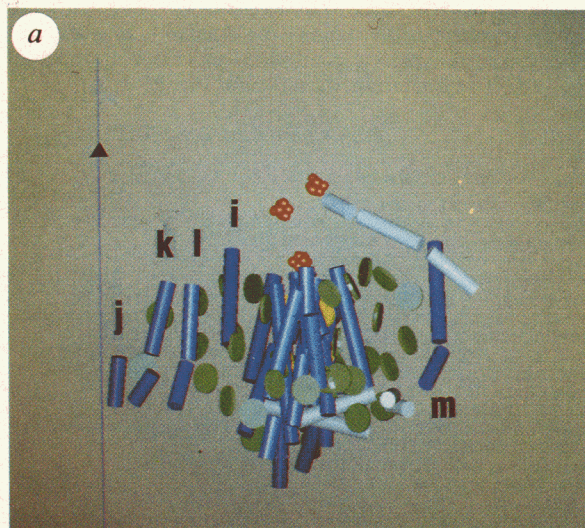


FIG 2 *a*, Section of the electron density map of a PS I monomer with view direction as in Fig. 1*c*, left. Shown is a slab containing the crystallographic 3-fold axis (yellow line). The blue contours are at a level 1.2 r.m.s. deviations above the mean density. The yellow contours (10 r.m.s. deviations) indicate the positions of the three iron-sulphur clusters. *b*, Elements of the electron density map fitted with polyaniline α -helices and the dihydroporphyrin of chlorophyll *a*. *c*, Section of the electron density map of the electron transfer chain. For the assignments see text. The two white dots indicate possible alternative positions for vitamin K_1 . Contours in *b*, *c* are at the same level as the blue one in *a*.

FIG. 3 Arrangement of structural elements in the PS I monomer pictured with the graphics program O⁵². The crystallographic 3-fold axis is indicated by \blacktriangle . *a*, View direction as in Fig. 1*c*, left. Transmembrane helices are shown as blue, and horizontal helices as white cylinders. Head groups of the antenna chlorophylls are shown as green disks, electron carriers in yellow. F_X , F_A , F_B are indicated as red spheres. Stroma is 'above', lumen 'below' the PS I complex. *b*, As *a*, but rotated 90° about the vertical. *c*, As *a*, but rotated 90° about the horizontal. The stromal side is toward the viewer. *d*, Same as *c*, but for clarity the chlorophylls and helices which are not of the transmembrane type (with the exception of *n* and *n'*) have been omitted. The local roughly 2-fold axis that relates helices *a* to *h* and *a'* to *h'* in subunits A and B is indicated by \bullet . For the letters see text.



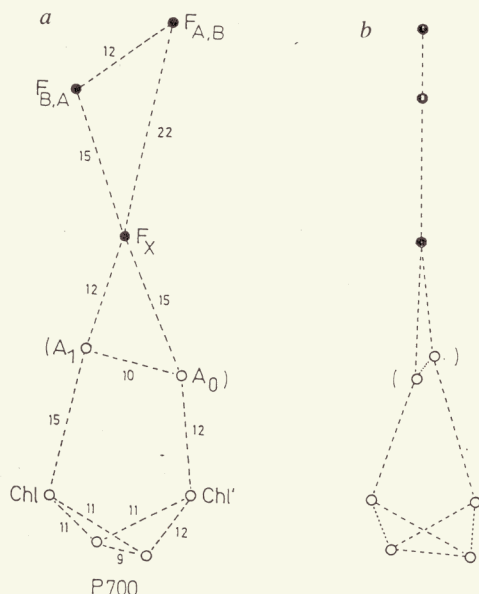


FIG. 4 *a*, Arrangement of the geometrical centres of the electron carriers shown in Fig. 2c (distances in Å). View direction is perpendicular to the plane defined by F_X , F_A , F_B . The local roughly 2-fold axis is vertical and passes through F_X . The open circles are meant to indicate the tentative character of the assignments. *b*, Same view as above, but rotated 90° about the vertical.

chains running between the stromal and luminal sides of PS I. Half of the possibly 90 chlorophyll *a* molecules have been located; 12 to 16 β -carotene molecules considered to be located in the A and B subunits¹² could not be identified.

The electron transfer chain

Of particular interest is the electron transfer chain (Figs 2c and 4). Because charge separation is directed across the photosynthetic membrane³⁵, P700 and the different electron acceptors are expected to form a chain extending from the luminal to the stromal side of PS I. The positions of the terminal acceptors in this chain, the three iron-sulphur centres, could be determined unambiguously; as a consequence, we anticipated that the other electron carriers are located in the region between F_X and the luminal surface of PS I, and close to the local 2-fold axis passing through F_X .

The charge separation is initiated at the primary electron donor P700, which might be a chlorophyll *a* dimer⁹⁻¹². In the electron density map (Fig. 2c), two chlorophylls located close to the 2-fold rotation axis are tentatively attributed to P700. Their centres are 9 Å apart (Fig. 4). The dihydroporphyrin plane of one of these two molecules is clearly oriented perpendicular to the membrane plane, but the orientation of the second chlorophyll *a* cannot be determined as the corresponding electron density is almost spherical. The orientation shown in Fig. 2c would agree with electron paramagnetic resonance (EPR) measurements, which indicate that P700 is oriented perpendicular to the photosynthetic membrane³⁶.

The predicted locus of P700 is close to the innermost tip of a distinct 10 Å indentation (Fig. 1c) of the luminal surface of the PS I complex and separated from it by the two α -helices (n, n') (Fig. 3d). This would be the place to dock plastocyanin. On one side of this docking site, the electron density map is characterized by disordered protein. This appears to be the location of the 15.1K subunit F, which was found by cross-linking studies to interact with plastocyanin³⁷.

Two ellipsoidal electron densities in the vicinity of P700 are possibly additional chlorophyll *a* molecules, Chl and Chl', which as yet have not been considered in the electron transfer chain. The centres of these dihydroporphyrins are ~11 Å from the P700 chlorophyll *a* and their planes are strongly inclined towards the normal of the membrane (Fig. 2c). This arrangement of the P700 dimer and two Chl and Chl' shows similarities to the RC of the purple bacteria².

Farther 'up' the chain, there is electron density which might be assigned to the electron acceptor A_0 (a chlorophyll *a*). About

10 Å away from A_0 , there is less extensive electron density that corresponds more closely to the naphthoquinone head group of A_1 (vitamin K_1). Two features in the electron density map at the locus indicated by white dots (Fig. 2c) possibly represent alternative positions for two vitamin K_1 molecules.

The distances between the putative electron carriers (Fig. 4a, b) predict a unidirectional P700- A_0 - A_1 - F_X - $F_{A,B}$ electron transfer with F_X as unambiguous intermediate. This was recently supported by an analysis of the kinetics of the reduction of F_X , which is independent of the presence and absence of $F_{A,B}$ ³⁸.

It must be stressed that our interpretation is tentative and thus at the present level of resolution an unambiguous decision on the arrangement of the electron carriers located between P700 and F_X is not possible. This refers especially to our assignment of electron densities to A_0 and A_1 and to the notion that there are in fact two vitamin K_1 molecules in PS I¹³. □

Received 2 November 1992; accepted 8 January 1993.

1. Witt, H. T. *New J. Chem.* **11**, 91-101 (1987).
2. Deisenhofer, J., Epp, O., Miki, K., Huber, R. & Michel, H. *Nature* **318**, 618-624 (1985).
3. Deisenhofer, J. & Michel, H. *EMBO J.* **8**, 2149-2170 (1989).
4. Trebst, A. *Z. Naturforsch.* **41c**, 240-245 (1986).
5. Mathis, P. *Biochim. biophys. Acta* **1018**, 163-167 (1990).
6. Nitschke, W., Feiler, U., Lockau, W. & Hauska, G. *FEBS Lett.* **218**, 283-286 (1987).
7. Mühlhoff, U., Haehnel, W., Witt, H. T. & Herrmann, R. G. *Nucleic Acids Res.* (in the press).
8. Mühlhoff, U. thesis, Technische Universität Berlin (1991).
9. Döring, G., Bailey, J., Kreutz, W., Weikard, J. & Witt, H. T. *Naturwiss.* **55**, 219-220 (1968).
10. Norris, J. R., Uphaus, R. A., Crespi, H. G. & Katz, J. J. *Proc. natn. Acad. Sci. U.S.A.* **68**, 625-629 (1971).
11. Philipson, K. D., Sato, V. L. & Sauer, K. *Biochemistry* **11**, 4591-4595 (1972).
12. Golbeck, J. H. & Bryant, D. A. *Curr. Topics Bioenerg.* **16**, 83-177 (1991).
13. Shuvalov, V. A., Nuijs, A. M., van Gorkom, H. J., Smit, H. W. J. & Duysens, L. M. N. *Biochim. biophys. Acta* **850**, 319-329 (1986).
14. Biggins, J. & Mathis, P. *Biochemistry* **27**, 1494-1500 (1988).
15. Brettel, K. *Biochim. biophys. Acta* **976**, 246-249 (1989).
16. Wynn, R. M. & Malkin, R. *FEBS Lett.* **229**, 293-297 (1988).
17. Mehari, T., Parett, K. G., Warren, P. V. & Golbeck, J. H. *Biochim. biophys. Acta* **1056**, 139-148 (1991).
18. Ford, R. C., Picot, D. & Garavito, R. M. *EMBO J.* **6**, 1581-1586 (1987).
19. Witt, I. et al. *FEBS Lett.* **221**, 260-264 (1987).
20. Ford, R. C., Pauptit, R. A. & Holzenburg, A. *FEBS Lett.* **238**, 385-389 (1988).
21. Witt, I. et al. *Ber. Bunsenges. Phys. Chem.* **92**, 1503-1506 (1988).
22. Shoham, G., Michaeli, D. & Nechushtal, R. *Current Research in Photosynthesis* vol. 2 (ed. Baltscheffsky, M.) 7555-7562. (Kluwer, Dordrecht, 1990).
23. Almog, O., Shoham, G., Michaeli, D. & Nechushtal, R. *Proc. natn. Acad. Sci. U.S.A.* **88**, 5312-5316 (1991).
24. Witt, H. T. et al. *Research in Photosynthesis* **1**, (Proc. IX Int. cong. Photosynthesis, Nagoya, Japan (ed. Murata, N.) 521-528 (Kluwer, Dordrecht, 1992).
25. McDermott, A. E. et al. *Biochemistry* **27**, 4013-4020 (1988).
26. Scheller, H. V., Svendsen, I. & Lindberg-Møller, B. *J. Biol. Chem.* **264**, 6929-6934 (1989).
27. Petrouleas, V., Brand, J. J., Parett, K. G. & Golbeck, J. M. *Biochemistry* **28**, 8980-8983 (1989).
28. Adman, E. T., Sieker, L. C. & Jensen, L. H. *J. Biol. Chem.* **248**, 3987-3996 (1973).
29. Oh-oka, H., Takahashi, Y., Kuriyama, K., Saeki, K. & Matsubara, H. *J. Biochem.* **103**, 962-968 (1988).
30. Moser, C. C., Keske, J. M., Warnocke, K., Farid, R. S. & Dutton, P. L. *Nature* **355**, 796-802 (1992).
31. Hiller, R. G., Bardin, A.-M. & Nabedryk, E. *Biochim. biophys. Acta* **894**, 365-369 (1987).
32. Kühlbrandt, W. & Wang, D. N. *Nature* **350**, 130-134 (1991).
33. Haworth, P., Tapie, P., Arntzen, J. & Breton, J. *Biochim. biophys. Acta* **682**, 152-159 (1982).
34. Matthews, B. W., Fenna, R. E., Bolognesi, M. C., Schmid, M. F. & Olson, J. M. *J. molec. Biol.* **131**, 259-285 (1979).
35. Junge, W. & Witt, H. T. *Z. Naturforsch.* **23b**, 244-254 (1968).
36. Rutherford, A. W. & Setif, P. *Biochim. biophys. Acta* **1019**, 128-132 (1990).
37. Hippler, M., Ratajczak, R. & Haehnel, W. *FEBS Lett.* **250**, 280-284 (1989).
38. Lüneberg, J. thesis, Technische Universität Berlin (1992).
39. CCP4, The Co-operative Computing Project in Crystallography (SERC Daresbury Laboratory, Warrington, UK, 1986).
40. Messerschmidt, A. & Pflugrath, J. W. *J. appl. Crystallogr.* **20**, 306-315 (1987).
41. Wang, B. C. *Meth. Enzym.* **114**, 472-475 (1985).
42. Leslie, A. G. W. *Acta crystallogr.* **A43**, 134-136 (1987).
43. Jones, A. T. *J. appl. Crystallogr.* **11**, 268-272 (1978).

-
44. Yeates, T. O., Komyia, H., Rees, D. C., Allen, J. P. & Feher, G. *Proc. natn. Acad. Sci. U.S.A.* **84**, 6438-6442 (1987).
45. Boekema, E. J. *et al.* *FEBS Lett.* **217**, 283-286 (1987).
46. Ford, R. C. & Holzenburg, A. *EMBO J.* **7**, 2287-2293 (1988).
47. Ford, R. C., Hefti, A. & Engel, A. *EMBO J.* **9**, 3067-3075 (1990).
48. Rögner, M., Mühlenhoff, U., Boekema, E. J. & Witt, H. T. *Biochim. biophys. Acta* **1015**, 415-424 (1990).
49. Böttcher, B., Gräber, P. & Boekema, E. J. *Biochim. biophys. Acta* (in the press).
50. Hladik, J. & Sofrova, D. *Photosynth. Res.* **29**, 171-175 (1991).
51. Hladik, J., Pospisilova, L. & Sofrova, D. *Current Research in Photosynthesis* Vol. 2 (ed. M. Baltscheffsky) 579-582 (Kluwer, Dordrecht, 1990).
52. Jones, T. A., Zou, J.-Y., Cowan, S. W. & Kjeldgaard, N. *Acta crystallogr.* **A47**, 110-119 (1991).

ACKNOWLEDGEMENTS. We thank W. Hæhnel for discussion and D. Di Fiore, Claudia Otto and I. Geisenheimer for technical support. This work was supported by the Deutsche Forschungsgemeinschaft through the Sonderforschungsbereich (W.S. and H.T.W.), through the Leibniz-Programm (W.S.), and by the Fonds der Chemischen Industrie (W.S. and H.T.W.).